



# Electronic transport through metal–1,4-phenylene diisocyanide–metal junctions

J. Chen <sup>a,\*</sup>, L.C. Calvet <sup>a</sup>, M.A. Reed <sup>a</sup>, D.W. Carr <sup>b</sup>, D.S. Grubisha <sup>c</sup>,  
D.W. Bennett <sup>c</sup>

<sup>a</sup> *Departments of Electrical Engineering, Applied Physics and Physics, Yale University, New Haven, CT 06520-8284, USA*

<sup>b</sup> *Cornell Nanofabrication Facility, Cornell University, Ithaca, NY 14852, USA*

<sup>c</sup> *Department of Chemistry, University of Wisconsin - Milwaukee, Milwaukee, WI 53211-3029, USA*

Received 22 July 1999; in final form 9 September 1999

## Abstract

We report measurements on through-bond electronic transport properties of 1,4-phenylene diisocyanide–metal junctions. Nanoscale metal–molecule–metal junctions with self-assembled 1,4-phenylene diisocyanide layers were analyzed with variable temperature conductance measurements to reveal the dominant electronic transport mechanisms. Non-Ohmic thermionic emission is the dominant process, with isocyanide–Pd showing the lowest thermionic barrier of 0.22 eV. © 1999 Elsevier Science B.V. All rights reserved.

## 1. Introduction

Electron transport studies in molecular-scale systems have recently become possible with the utilization of advanced microfabrication and self-assembly techniques [1]. Self-assembled monolayers (SAMs) of oligomers onto metals are well known, the most widely studied system being the Au–SR system (R = alkyl), which forms a very well-ordered single monolayer with an aggressive  $\sim 2$  eV bond [2–6]. Investigations of the electronic conduction through conjugated molecules that are end-bound onto surface are now possible, and has been demonstrated with a scanning tunneling microscope (STM) [7], micromachined silicon nanopores [8], and between

proximal probes [9,10]. Although a good deal is known about the structural properties of various functional terminal moieties on both aliphatic and aromatic molecules, very little is known about the electrical properties of through-bond transport. At present, the only through-bond system measured has been Au–thiol [8]. Here we present data on a second type of molecule–metal junction, specifically 1,4-phenylene diisocyanide with metal (Au or Pd) contacts. This system has significant electronic advantages over the thiol and other Group VI systems (e.g., Se, Te).

To understand the electrical conduction of a metal–molecule system, the energetic matching (or, mismatching) of the available electrons in the metal (the Fermi level) and the available molecular orbital in the terminal molecule must be considered. In general, the Fermi level of the metallic contact does

\* Corresponding author. Fax: +1-203-432-6420; e-mail: jia.chen@yale.edu

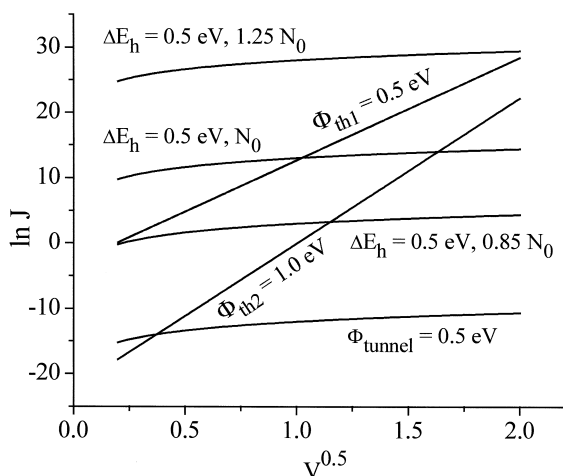


Fig. 1. Dependencies of  $\ln J$  vs.  $V^{1/2}$  for thermal emission, hopping, and tunneling transport. The effect on thermionic emission for two different barrier heights is shown; for  $\Phi_{th2}(1.0 \text{ eV}) > \Phi_{th1}(0.5 \text{ eV})$ , the thermionic emission component drops (exponentially). The effect of defect (e.g., hopping) conduction is shown for different defect densities ( $1.25 N_0 > N_0 > 0.85 N_0$ ) even though the hopping barrier may be the same ( $\Delta E_h = 0.5 \text{ eV}$ ). Tunneling component (with  $\Phi_{tunnel} = 0.5 \text{ eV}$ ) is much smaller than the others. Depending on the value of  $\Phi_{th}$ ,  $\Delta E_h$ ,  $N$ , and  $\Phi_{tunnel}$  one may observe different mechanisms; e.g., both are observable for  $\Phi_{th1}$  and  $N_0$ , if  $\Delta E_h = \Phi_{th1}$ .

not energetically line up with either the HOMO or LUMO levels in the molecule [11]. This mismatch gives rise to a contact barrier, analogous to a Schottky contact. Electron (or hole) transport through such a contact will exhibit a range of phenomena, depending on the size of the barrier, the effective barrier thickness, and the presence of defects; the most prevalent are thermionic emission, direct tunneling, and defect-mediated transport such as hopping [12–14]. Fig. 1 shows the  $I(V)$  dependencies of these mechanisms for various barrier heights, which can be used to elucidate the dominant specific mechanism and effective barriers.

## 2. Experiment

To reliably measure a molecule–metal barrier system, we employ a novel fabrication technique to directly measure the conduction through a small number of self-assembled molecules sandwiched be-

tween top and bottom metallic contacts [8]. This technique guarantees good control over the device area and intrinsic contact stability, and produces a large number of devices with acceptable yield so that statistically significant results can be produced. Two essential features are essential to the process, the first of which is the employment of nano-scale device area. The area is made to be smaller than the domain size of the SAM and thus the adsorbed organic layer is highly ordered and (mostly) defect free. The second feature is that during the deposition (evaporation) of the contact onto the SAM, several measures are taken to ensure that the deposited metal atoms accumulate at the SAM surface and do not penetrate into the organic layer. These methods also provide minimized damage to the SAM during the deposition. Fig. 2 is a schematic of the device structure used, of which the details of the fabrication have been reported previously [8]. The starting substrate is a  $250 \mu\text{m}$  thick (100) double-sided polished silicon wafer, upon which  $50 \text{ nm}$  of low-stress  $\text{Si}_3\text{N}_4$  is deposited by low-pressure chemical vapor deposition (LPCVD). On the back surface, the nitride is removed in a  $(400 \mu\text{m} \times 400 \mu\text{m})$  square by optical lithography and reactive ion etching (RIE). The exposed silicon is etched in an orientation-dependent anisotropic etchant ( $85^\circ\text{C}$  35% KOH solution) through to the top surface, leaving a suspended  $(40 \mu\text{m} \times 40 \mu\text{m})$  silicon nitride membrane.  $1000 \text{ \AA}$   $\text{SiO}_2$  was thermally grown on the Si sidewalls to improve electrical insulation. A single hole of size  $30\text{--}50 \text{ nm}$  is made through the membrane by electron beam lithography and RIE. Because of the constrained geometry, the RIE rates are substantially reduced so that the far side opening is much smaller than that actually patterned rendering the cross-section bowl-shaped geometry<sup>1</sup> [15]. A Au contact of  $200 \text{ nm}$  thickness was evaporated onto the top side of the membranes, which filled the pore with Au. The sample was then transferred immediately into  $1 \text{ mM}$  1,4-phenylene diisocyanide in toluene (Aldrich) under an Ar atmosphere. The self-assembly of diisocyanide [16,17] onto the gold substrate was allowed for  $48 \text{ h}$  under an inert atmosphere of Ar. The

<sup>1</sup> Note that the process employed here was slightly modified (the bowl is inverted) over that employed in Ref. [4].

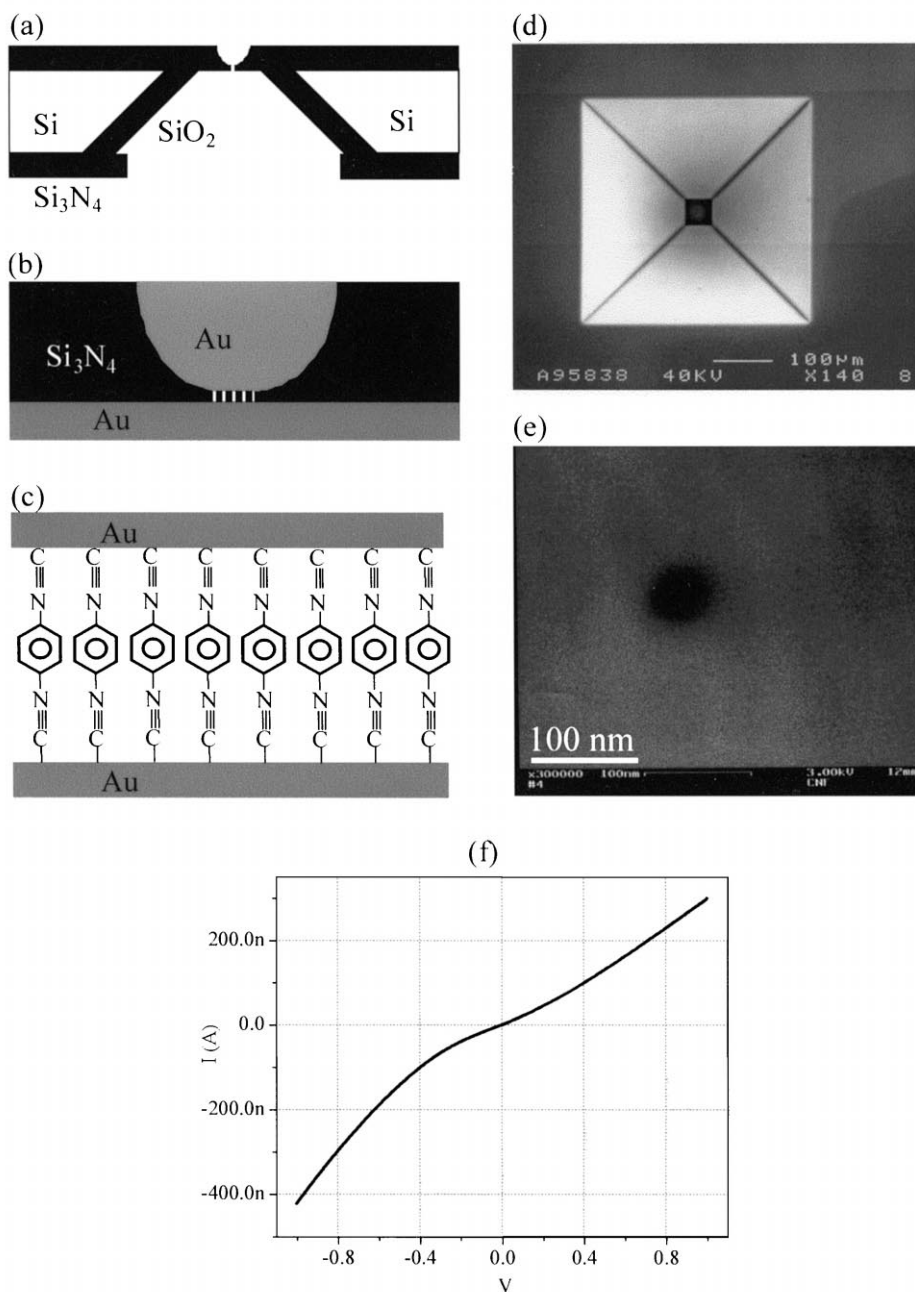


Fig. 2. Schematics of device fabrication: (a) cross-section of a silicon wafer with a nanopore etched through a suspended silicon nitride membrane; (b) Au-SAM-Au junction in the pore area; (c) blowup of (b) showing 1,4-phenylene diisocyanide sandwiched in the junction; (d) scanning electron microscope (SEM) picture of pyramid Si structure after anisotropic Si etching; (e) SEM micrograph of an etched nanopore through silicon nitride membrane; and (f)  $I(V)$  of Pd-SAM-Pd junction at 290 K.

sample was then rinsed and quickly loaded into a vacuum chamber and mounted onto a liquid-nitrogen cooling stage for the opposing gold electrode evaporation, where 200 nm Au was evaporated at 77 K at a rate of  $< 1 \text{ \AA/s}$ . The devices were then diced into individual chips, bonded onto packaging sockets and loaded into a variable-temperature cryostat (Janis) and measured with a HP4145 Semiconductor Parameter Analyzer (SPA). A series of control experiments have been done using alkanethiol molecules, silicon nitride membranes without pores and membranes with pores but without molecules, respectively. Both the Au–alkanethiol–Au junctions and the Au–silicon nitride membrane–Au junctions showed current levels at the noise limit of the apparatus ( $< 1 \text{ pA}$ ) for both bias polarities at both room and low temperatures. The Au–Au junctions gave Ohmic  $I(V)$  characteristics with resistances of  $< 2 \text{ \Omega}$ .

### 3. Results and discussion

Previous work on self-assembled thiol-terminated (but asymmetric) oligomers illustrated that one can deduce the basic transport mechanisms (illustrated in Fig. 1) by measuring the  $I(V, T)$  characteristics. In the previous work, it was found that the physisorbed aryl–Ti interface gave a thermionic emission barrier

of  $\sim 0.25 \text{ eV}$  [8], whereas the Au–thiol (and other Group VI termini such as Se and Te) bond exhibited a hopping barrier of  $\sim 0.2 \text{ eV}$  [18]. Surprisingly, this is consistent with other transport measurements on a single molecule [9] that implied a barrier of  $\sim 0.7 \text{ eV}$ , since the current from the  $0.2 \text{ eV}$  defect-mediated hopping barrier (not present in the single-molecule experiment) is significantly larger than that from the  $0.7 \text{ eV}$  barrier. It should be noted that such an asymmetric contact structure is useful to create large rectification characteristics arising simply from the different contact potentials (versus the more complicated *zwitterionic* mechanism [19,20]); symmetric structures should not (and do not) show such rectification, as seen in this study (Fig. 2f).

In this work, we investigate two new aspects of through-bond electronic conduction in the nanopore configuration, namely: (a) the transport through the self-assembled functional termini of isocyanide, and its effective electron transport barrier; and (b) a symmetric termini-metal contact structure. To determine the effective transport characteristics,  $I(V, T)$  measurements are performed from 300 to 4 K with voltage swept between  $-1$  and  $+1 \text{ V}$ . Fig. 3a illustrates reduced  $I(T)$  characteristics at various voltages when the junction is biased in the direction that electrons are injected from the chemisorbed Au–isocyanide contact; one sees that the dependence

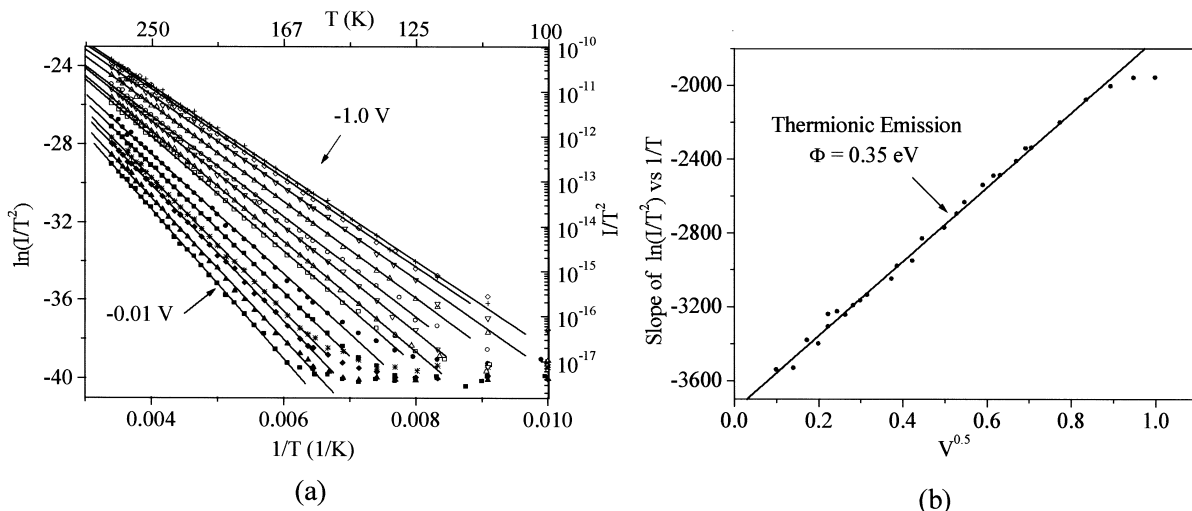


Fig. 3. Au–SAM–Au junction: (a) series of plots of  $\ln(I/T^2)$  vs.  $1/T$  at biases from  $-0.01$  to  $-1.0 \text{ V}$ ; (b) plot of the slope of  $\ln(I/T^2)$  vs.  $1/T$  vs.  $V^{0.5}$  shows a linear dependence. Thermal barrier height of the Au–SAM–Au junction can be deduced from the interception of the straight line. All the straight lines are  $\chi^2$  fits for respective data sets.

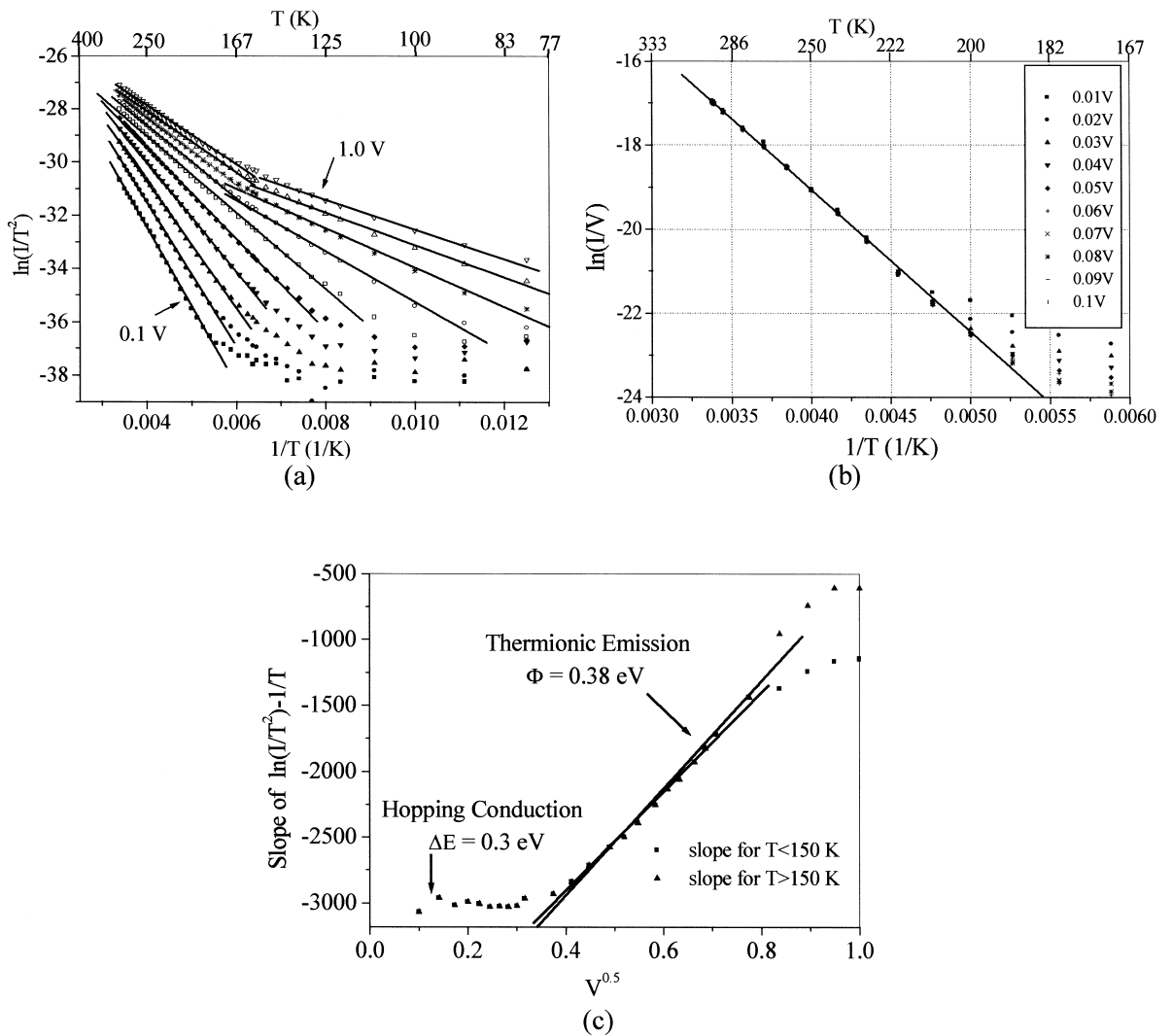


Fig. 4. Au–SAM–Au junction: (a) series of plots of  $\ln(I/T^2)$  vs.  $1/T$  at biases from 0.1 to 1.0 V at 0.1 V increment; (b)  $\ln(I/V)$  vs.  $1/T$  at biases less than 0.1 V; and (c) plot of the slope of  $(\ln(I/T^2)$  vs.  $1/T)$  vs.  $V^{0.5}$ ; at  $0 < V < 0.1$  V, no bias dependence; at  $V > 0.1$  V, linear dependence. Thermal barrier height of the Au–SAM–Au junction can be deduced from the interception of the straight line. All the straight lines are  $\chi^2$  fits for respective data sets.

of  $\ln(I/T^2)$  vs.  $1/T$  ( $-0.01$  to  $-1$  V) has a clear linear dependence. This dependence is characteristic of thermionic emission [13,14], where

$$I = A^* T^2 \exp\left(-\frac{q\Phi - a\sqrt{V}}{kT}\right),$$

$$a = q\sqrt{\frac{q\Phi}{4\pi\epsilon_0\epsilon d}},$$

where  $A^*$  is the effective Richardson constant multiplied by the current injection area,  $\Phi$  the thermal emission barrier height,  $k$  is Boltzmann’s constant,  $q$  the electron charge,  $\epsilon_0$  the vacuum dielectric constant,  $\epsilon$  the relative dielectric constant of the SAM, and  $d$  the thickness of the film. The barrier height was determined in Fig. 3b, where the slope of  $(\ln(I/T^2)$  vs.  $1/T)$  was plotted against  $V^{0.5}$ . The interception of the line fit gives a thermionic barrier

of  $\Phi = 0.35 (\pm 0.01)$  eV. When the junction is biased in the reverse direction such that electrons are injected from the evaporated Au–isocyanide contact, similar activation behavior was observed above 0.1 V (Fig. 4a). For  $V > 0.7$  ( $E \approx 7$  MV/cm), deviation from a linear dependence is observed and is probably due to high-field breakdown effects. Below 0.1 V, the dependence does not have the voltage dependence characteristic of thermionic emission, and in-

stead one finds a linear dependence of  $\ln(I/V)$  vs.  $1/T$ . This dependence is characteristic of hopping conduction, where

$$\ln(I/V) = f(N) - \Delta E/(kT),$$

where  $\Delta E$  is the activation energy to hop from one site to another and  $f(N)$  is a function of the trap concentration [14]. Fig. 4b shows this dependence in the regime of bias less than 0.1 V. Whereas the

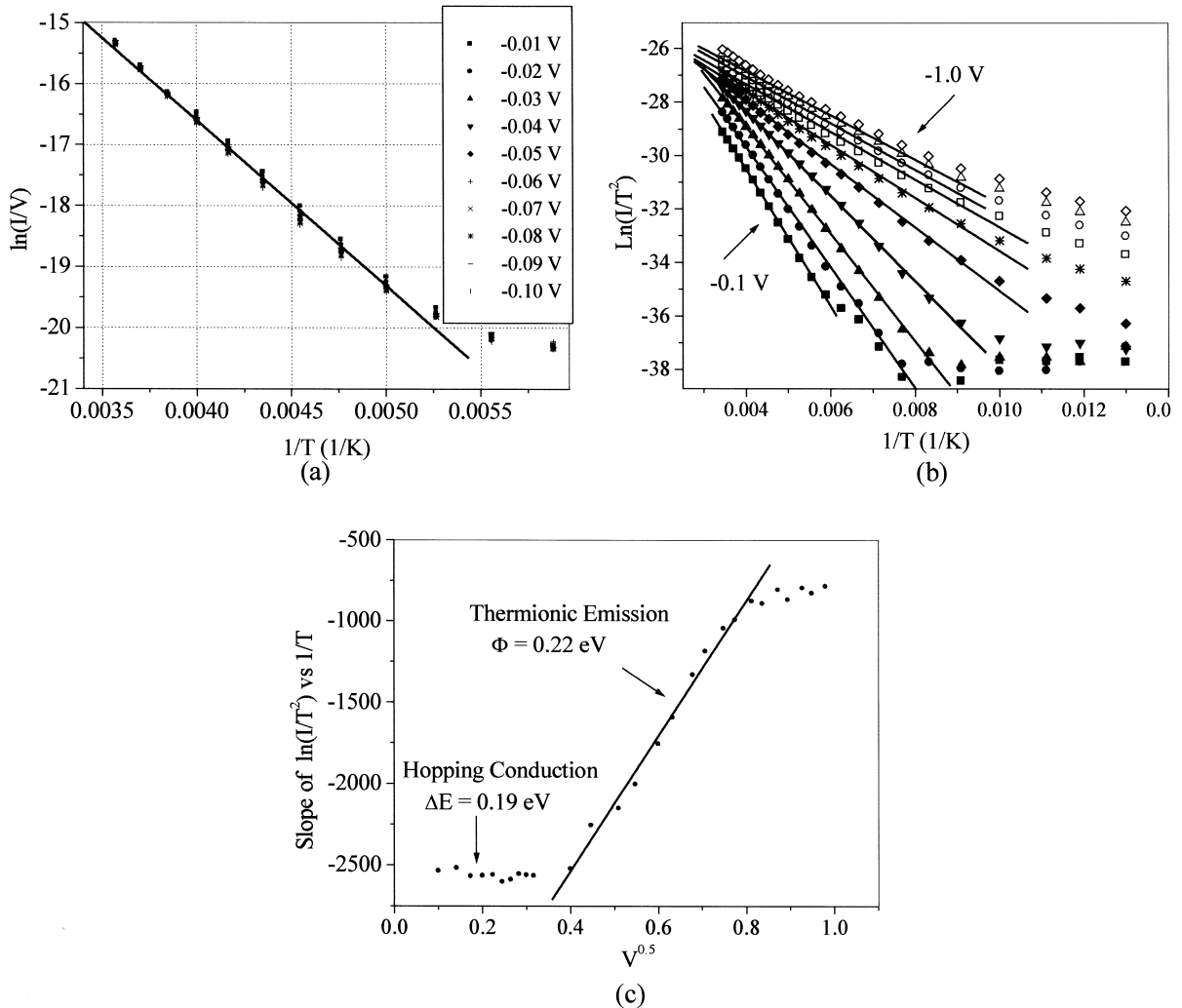


Fig. 5. Pd–SAM–Pd junction: (a)  $\ln(I/V)$  vs.  $1/T$  at biases larger than  $-0.1$  V; (b) series of plots of  $\ln(I/T^2)$  vs.  $1/T$  at biases from  $-0.1$  to  $-1.0$  V at  $-0.1$  V increment; and (c) plot of the slope of  $\ln(I/T^2)$  vs.  $1/T$  vs.  $V^{0.5}$ : at  $-0.1$  V  $< V < 0$ , no bias dependence; at  $V < -0.1$  V, linear dependence. Thermal barrier height of the Pd–SAM–Pd junction can be deduced from the interception of the straight line. All the straight lines are  $\chi^2$  fits for respective data sets.

physical interpretation of the thermionic transport barrier is clearly the molecule–metal contact potential, the physical sites giving rise to hopping transport is less well defined. Structural defects in the nanopore, or edge defects are potential candidates for the low-bias defect-mediated transport.

To determine the energetic barriers, we plot the slope of  $(\ln(I/T^2) \text{ vs. } 1/T) \text{ vs. } V^{0.5}$  in Fig. 4c). For the isocyanide–Au contact, we obtain for  $0 \text{ V} < V < 0.1 \text{ V}$ , a hopping barrier of  $\Delta E = 0.3 (\pm 0.01) \text{ eV}$ ; and for  $0.1 \text{ V} < V < 1 \text{ V}$ , a thermionic emission barrier  $\Phi = 0.38 (\pm 0.01) \text{ eV}$ . As schematically denoted in Fig. 1, the observation of the various mechanisms in a given junction will depend on both the magnitude of the various barriers and the defect density. For negative bias, we only observe thermionic emission, with an unobservable defect component. For positive bias, the defect component is larger, and we observe both simultaneously. (We note that if the thermionic emission barrier is too large, such as in the case of thiol-like termini onto Au, only the hopping barrier would be observable.) As defect-mediated conduction is a complicated function of trap concentration and details, a significantly more extensive study would be necessary to elucidate the nature and effects of process on the defects. The present study serves to identify the characteristic energy, although the origin and density (and thus the current magnitude) is not well controlled.

Because the fabrication technique is generalizable to different termini and metals, it is easy to compare the effects of different contacts. Utilizing the same fabrication technique but instead substituting the metal Au with Pd, Pd–1,4-phenylene diisocyanide–Pd junctions were fabricated and measured as before. Fig. 5 shows plots of: (a)  $\ln(I/V) \text{ vs. } 1/T$  (low bias), illustrating hopping conduction when electrons

were injected from the chemisorbed Pd–isocyanide contact; and (b)  $\ln(I/T^2) \text{ vs. } 1/T$  (high bias), illustrating thermionic emission. Fig. 5c illustrates the slope of  $(\ln(I/T^2) \text{ vs. } 1/T) \text{ vs. } V^{0.5}$  at negative bias, and we obtain: (a) for  $-0.1 \text{ V} < V < 0 \text{ V}$ , a hopping barrier of  $\Delta E = 0.19 (\pm 0.02) \text{ eV}$ ; for  $V < -0.1 \text{ V}$ , a thermionic emission barrier  $\Phi = 0.22 (\pm 0.02) \text{ eV}$ . In this case, the unidentified defect component was large such that both thermionic and hopping are observed. When electrons are injected from the evaporated Pd–CN contact, the defect component was so large that only hopping is observed.

#### 4. Conclusions

Table 1 summarizes the results of the transport barriers of through-bond transport of isocyanide on the metals measured in this study. It is observed that thermal emission is the dominant conduction mechanism in chemisorbed metal–isocyanide junctions, while in the evaporated metal–isocyanide contact, both hopping and thermal emission can play an important role depending on the defect level introduced during the fabrication process. The barriers of both the chemisorbed and the evaporated contact are approximately the same, which is expected given the symmetry of the structure. It appears that the hopping component in the chemisorbed metal–molecule junction is less significant than that in the evaporated metal–molecule junction. Overall, the Pd–CN contact barrier is smaller than that of a Au–CN junction. The technique reported here elucidates the relevant electronic transport barriers and conduction mechanisms of through-bond metal–molecule contacts, which have been possible through the implementation of microfabricated electronic devices utilizing SAMs. The technique should be applicable to a large

Table 1  
Summary of the barriers and conduction mechanisms for various metal/SAM interfaces

Metal	Au	Pd
Chemisorbed contact	0.35 eV, thermionic	0.22 eV, thermionic (0.19 eV hopping at low bias)
Evaporated contact	0.38 eV, thermionic (0.3 eV hopping at low bias)	0.21 eV, hopping

range of inorganic and biomolecular transport measurements, to quantitatively measure the dominant electron transport mechanisms.

### Acknowledgements

The authors would like to thank Michael Rooks, Mandar Deshmuke, and Nicole Wagner for stimulating discussions. This work was supported by DARPA.

### References

- [1] A. Aviram, M. Ratner, *Molecular Electronics: Science and Technology*, Ann. NY Acad. Sci. (1998).
- [2] P.E. Laibinis, G.M. Whitesides, D.L. Allara, A. Parikh, Y.T. Tao, R.G. Nuzzo, *J. Am. Chem. Soc.* 113 (1991) 7152.
- [3] C.D. Bain, J. Evall, G.M. Whitesides, *J. Am. Chem. Soc.* 111 (1989) 7155.
- [4] J.I. Henderson, S. Feng, G.M. Ferrence, T. Bein, C.P. Kubiak, *Inorg. Chim. Acta* 242 (1996) 115.
- [5] J.J. Hickman, C. Zou, D. Offer, P.D. Harvey, M.S. Wrighton, P.E. Laibinis, C.D. Bain, G.M. Whitesides, *J. Am. Chem. Soc.* 111 (1989) 7271.
- [6] J.M. Tour, L. Jones II, D.L. Pearson, J.S. Lamba, T.P. Burgin, G.M. Whitesides, D.L. Allara, A.N. Parikh, S. Atre, *J. Am. Chem. Soc.* 117 (1995) 9529.
- [7] L.A. Bumm, J.J. Arnold, M.T. Cygan, T.D. Dunbar, T.P. Burgin, L. Jones II, D.L. Allara, J.M. Tour, P.S. Weiss, *Science* 271 (1996) 1705.
- [8] C. Zhou, M.R. Deshpande, M.A. Reed, L. Jones II, J.M. Tour, *Appl. Phys. Lett.* 71 (1997) 611.
- [9] M.A. Reed, C. Zhou, C.J. Muller, T.P. Burgin, J.M. Tour, *Science* 278 (1997) 252.
- [10] C. Kergueris, J.-P. Bourgoin, S. Palacin, D. Esteve, C. Urbina, M. Magoga, C. Joachim, *Phys. Rev. B* 59 (1999) 12505.
- [11] S. Datta, W. Tian, S. Hong, R. Reifenberger, J. Henderson, C.P. Kubiak, *Phys. Rev. Lett.* 79 (1997) 2530.
- [12] E. Burstein, S. Lundqvist, *Tunneling Phenomena in Solids*, Plenum, New York, 1969.
- [13] S.M. Sze, *Physics of Semiconductor Devices*, Wiley, New York, 1981.
- [14] D.R. Lamb, *Electrical Conduction Mechanisms in Thin Insulating Films*, Methuen, London, 1967.
- [15] K.S. Ralls, R.A. Buhrman, R.C. Tiberio, *Appl. Phys. Lett.* 55 (1989) 2459.
- [16] I. Ugi, U. Fetzer, U. Eholzer, H. Knupfer, K. Offerman, *Angew. Chem., Int. Ed. Engl.* 4 (1965) 472.
- [17] M.J. Robertson, R.J. Angelici, *Langmuir* 10 (1994) 1488.
- [18] C. Zhou, Ph.D. Thesis, Yale University, New Haven, CT, 1999.
- [19] A. Aviram, M.A. Ratner, *Chem. Phys. Lett.* 29 (1974) 277.
- [20] R.M. Metzger, B. Chen, U. Höpfner, M.V. Lakshmikantham, D. Vuillaume, T. Kawai, X. Wu, H. Tachibana, T.V. Hughes, H. Sakurai, J.W. Baldwin, C. Hosch, M.P. Cava, L. Brehmer, G.J. Ashwell, *J. Am. Chem. Soc.* 119 (1997) 10455.